Acta Pharm. **76**(2) (2026) 260015 (26 pages) Article
https://doi.org/10.2478/acph-2026-0015

Synergistic effect of piperine combined with luteolin on anti-non-small cell lung cancer activity *in vitro* and in LLC tumour-bearing mice: Mechanistic insights from network pharmacology and molecular docking

LIANGFENG WANG[1,2,3]
YUEXING CHANG[1,2,3,4,5,*]
YUFENG LIU[1,2,3]
AILING GUO[1,2,3,4]
BAORONG WANG[1,2,3]
FENG JIN[1,2,3]
YUN DENG[1,2,3]

[1] *School of Medicine, Anhui University of Science and Technology, Huainan 232001, China*

[2] *Key Laboratory of Industrial Dust Deep Reduction and Occupational Health and Safety of Anhui Higher Education Institutes, Huainan 232001, China*

[3] *Anhui Province Engineering Laboratory of Occupational Health and Safety Huainan 232001, China*

[4] *Key Laboratory of Tropical Medicinal Plant Chemistry of Hainan Province Hainan Normal University, Haikou 570100, China*

[5] *Analytical and testing center, Anhui University of Science and Technology Huainan 232001, China*

Accepted May 25, 2026
Published online May 26, 2026

ABSTRACT

Piperine had synergistic effects with other natural products in treating lung cancer. The synergistic effects of piperine combined with luteolin on anti-non-small cell lung cancer activity and their mechanism of action are studied using network pharmacology and molecular docking. Cell viability, wound-healing, colony-formation, cell-apoptosis, and cell-cycle tests on A549 cells were used to detect the *in vitro* synergistic effects. Tumour growth and hematoxylin and eosin (HE) staining were used to verify the synergistic effects in Lewis lung carcinoma (LLC) tumour-bearing mice. Their combination indexes ranged from 0.3 to 0.8 across different concentrations, and the combination of 175.3 μmol L^{-1} piperine and 87.32 μmol L^{-1} luteolin showed synergistic inhibition of A549 cell viability. Moreover, the combination induced a higher apoptosis rate (75.60 %) than luteolin (24.56 %) or piperine (17.53 %). It arrested more cells in the G0/G1 phase than luteolin or piperine did. The combination achieved a tumour inhibition rate of 75.28 %, with lower tumour density and more obvious apoptosis. Network pharmacology identified AKT1, EGFR, SRC, and MMP9 as core targets regulating the PI3K/AKT pathway. Multi-software molecular docking confirmed binding of both compounds to these targets, with MMP9 as the common primary target. In conclusion, piperine and luteolin acted synergistically against non-small cell lung cancer.

Keywords: luteolin, piperine, drug combination therapy, non-small cell lung cancer, network pharmacology, molecular docking

INTRODUCTION

Non-small cell lung cancer (NSCLC) was a major subtype of lung cancer (1), accounting for approximately 80–85 % of all lung cancer cases (2). Chemotherapy,

* Correspondence; e-mail: yxchang@aust.edu.cn

targeted therapy, and immunotherapy have played an important role in NSCLC treatment (3). However, there are still some shortcomings, such as drug resistance and high toxicity to normal cells (4). In fact, the combined application of natural products has begun to show promise in the treatment of early non-small cell lung cancer. The combination of curcumin and resveratrol regulated p53 hyperphosphorylation, enhanced caspase activity, and exerted a synergistic preventive effect on lung carcinogenesis (5). Coincidentally, the combination of curcumin and berberine also significantly inhibited MDR1 activity, promoted apoptosis of A549 lung cancer cells, and enhanced anti-lung cancer efficacy (6). Of course, there are still many unknown areas to be explored in the combination of natural products.

Luteolin is a natural flavonoid found in many plants, such as *Reseda odorata* L., *Lonicera japonica* Thunb., *Chrysanthemum morifolium* Ramat., and others (7). It has diverse biological activities, such as anti-inflammatory, antioxidant, antibacterial, anticancer, and antidiabetic properties (8–12). In particular, its anticancer effect has been closely studied. It was generally used to treat different cancers such as gastric cancer, colorectal cancer, breast cancer, liver cancer, and lung cancer. In particular, it has a marked inhibitory effect on lung cancer (13–17). In the treatment of lung cancer, luteolin inhibited the proliferation, migration, and invasion of A549 cells by regulating signalling pathways, including MEK/ERK and AKT/mTOR (18, 19). However, it has a weaker anti-lung cancer effect than other drugs such as osimertinib, sacituzumab govitecan, and pembrolizumab (20–22). Based on the above discussion, its anti-lung cancer effect may be improved by combining it with other natural products. Piperine enhanced the anticancer efficacy of several natural products, including curcumin, paclitaxel, and piperlongumine (23–26). In our preliminary experiments, preliminary experiments showed that piperine and luteolin had a combined effect in treating lung cancer. The combination of piperine and luteolin needs to be further verified, and their combined mechanism of action remains unclear.

Network pharmacology can incorporate information associated with drug components, targets, and diseases. From a holistic perspective, it forecasts drug-action mechanisms and provides a new perspective for natural medicine research (27). In contrast, molecular docking mimics drug-target interactions at the atomic scale, predicts binding affinities and modes, validates network pharmacology results, and accelerates mechanism analysis (28). Importantly, the crystal structures used for molecular docking in this study (PDB: 1GKC for MMP-9, 1M14 for EGFR, and 1FMK for SRC) have been successfully employed in previous cancer-related docking studies. For instance, Li *et al.* (29) used the MMP-9 structure (1GKC) to demonstrate that a novel phytosteroid saponin inhibits lung cancer cell migration *via* NF-κB-mediated MMP-2/MMP-9 suppression. Aggarwal *et al.* (30) employed the EGFR structure (1M14) to show that an organotin compound binds to the tyrosine kinase domain and exerts anticancer activity through inhibiting EGFR dimerisation. Jumaa *et al.* (31) used the SRC structure (1FMK) to show that a ciprofloxacin-metformin combination synergistically targets distinct SRC kinase sites in cervical cancer cells. These studies validate the suitability of the chosen PDB structures for docking investigations in the context of cancer therapy.

Therefore, in this study, we employed network pharmacology and molecular docking to explore the synergistic anti-NSCLC mechanisms of piperine and luteolin, with a focus on the validated targets EGFR, MMP9, and SRC. The synergistic effect was then determined by cell viability, wound healing, colony formation, apoptosis, and cell cycle assays on A549 cells, and further verified in Lewis lung carcinoma (LLC) tumour-bearing mice.

EXPERIMENTAL

Drugs and reagents

Piperine (purity ≥ 98 % HPLC; Shanghai Yuanye Biotechnology, China, Cat# T25317), luteolin (purity ≥ 98 % HPLC; Xi'an Tianbao Biotechnology, China), and the positive control drug gefitinib (purity ≥ 99 %; Shanghai Aladdin Biochemical Technology, China, Cat# G125799) were all dissolved in dimethyl sulfoxide (DMSO) to prepare stock solutions for experiments. Working concentrations were obtained by diluting the stocks in cell culture medium immediately before use. RPMI 1640 medium, DMEM medium, and 0.25 % trypsin were all obtained from Thermo Fisher Scientific Biochemical Products Co., Ltd. (China). Fetal bovine serum (FBS) was bought from Shanghai Shuangru Biotechnology Co., Ltd. (China). Penicillin-streptomycin solution was purchased from Shanghai Biyuntian Biotechnology Co., Ltd. (China). The Cell Apoptosis Detection Kit (KGA1101-50) and Cell Cycle Detection Kit (KGA9101-100) were both purchased from Jiangsu KeyGen Biotechnology Co., Ltd. (China).

Cell lines and experimental animals

A549 cells were gifted by Dr Tian Chang from Anhui University of Science and Technology (Anhui, China). They were cultured in RPMI 1640 medium supplemented with 10 % (*V*/*V*) FBS and 0.1 % (*V*/*V*) penicillin-streptomycin solution, and incubated in a humidified incubator at 37 °C with 5 % CO_2. A549 cells in logarithmic growth phase were harvested, prepared into a single-cell suspension, and used for cell detection experiments.

Lewis lung cancer (LLC) cells were purchased from Shanghai Institute of Biochemistry and Cell Biology (China). They were cultured in DMEM medium containing 10 % FBS under adherent conditions at 37 °C in a 5 % CO_2 atmosphere. They were used to prepare Lewis lung cancer (LLC) tumour-bearing mice. The A549 and LLC cell lines were authenticated by short tandem repeat (STR) profiling analysis. The STR profiles were consistent with the reference data from public databases (*e.g.,* ATCC, DSMZ), and no cross-contamination was detected.

Specific-pathogen-free (SPF) grade male C57BL/6J mice, 6 weeks old and weighing 20–22 g, were purchased from Hangzhou Ziyuan Laboratory Animal Co., Ltd., China (SCXK2024-0004). Mice were kept in a clean environment with a temperature of 25 ± 1 °C and a relative humidity of 50 ± 10 %. This experiment was approved by the Ethics Review Committee of Anhui University of Science and Technology (Gz2024-043). During the experiment, we strictly followed animal ethics requirements.

A combination of concentration selection and synergy evaluation

To evaluate the combination of piperine and luteolin, a fixed-ratio design based on the Chou-Talalay method was used. Concentrations below the individual 24 h half-maximal inhibitory concentration (IC_{50}) values were selected as the combined treatment doses. Specifically, luteolin was tested at three concentrations (87.32, 43.66, 21.83 μmol L^{-1}) and piperine at five concentrations (43.82, 87.64, 175.3, 280.4, 350.5 μmol L^{-1}), forming a 3×5 concentration matrix. All combinations were prepared such that each single-agent concentration

remained below its respective IC_{50}. Cells were treated for 24 h. The combination index (CI) was calculated using CompuSyn software (ComboSyn Inc., USA) according to the classic Chou-Talalay method (32). The combined effect was analysed using a dose-effect combination index (Fa-CI) and a normalised isobologram. The relationship between CI and the intensity of the synergistic effect is shown in Table I. In addition, cell morphology was observed at 0, 24, and 48 h after treatment and staining with sulforhodamine B (SRB), and the images were photographed using an Olympus IX73 microscope (Olympus Corporation, Japan).

Table I. Corresponding relationship between combination index (CI) values and evaluation of drug interactions (31)

Combination index value range	Interaction evaluation	Symbol
CI<0.10	Very strong synergism	+++++
0.10<CI<0.30	Strong synergism	++++
0.30<CI<0.70	Relatively strong synergism	+++
0.70<CI<0.85	Moderate synergism	++
0.85<CI<0.90	Slight synergism	+
0.90<CI<1.10	Additive effect	±
1.10<CI<1.20	Slight antagonism	–
1.20<CI<1.45	Moderate antagonism	––
1.45<CI<3.30	Relatively strong antagonism	–––
3.30<CI<10.00	Strong antagonism	––––
10.00<CI	Very strong antagonism	–––––

Wound healing assay

The scratch wound healing assay was used to evaluate the migration ability of A549 cells under different drug treatments. A549 cells of 3.5×10^5 cells mL^{-1} were seeded into a 96-well plate and incubated for 4 h. A sterile pipette tip was used to scratch vertically through the centre of the bottom of each well. Subsequently, A549 cells were treated with medium, luteolin, piperine, or the combination of piperine and luteolin in serum-free medium for 48 h. They were photographed at 0, 24, and 48 h, respectively. ImageJ software was used to calculate the wound-healing areas and the cell migration rate.

Colony formation assay

The colony formation assay was used to assess the A549 cell proliferation. A549 cells of 1.0×10^3 cells per mL were seeded in a 6-well plate. Subsequently, they were treated with medium, luteolin, piperine, or the combination of piperine and luteolin for 10 days. The medium was updated every 3 days. The cell clones were then fixed with trichloroacetic acid (TCA) and stained with SRB. They were photographed and numbered using ImageJ software.

Cell apoptosis assay

Annexin V-FITC/PI double-staining flow cytometry was used to detect the effects of different drug treatments on A549 cells. A549 cells of 2.0×10^5 cells mL^{-1} were seeded in a 6-well plate and treated with different drugs for 48 h. The apoptotic cells were detected by using an apoptosis detection kit (KGA1101-50, KeyGEN, China). Specifically, all cells were collected and incubated with a staining solution containing 5 μL of annexin V-FITC and 5 μL of propidium iodide (PI) in the dark at room temperature for 15 min. After that, they were detected using a flow cytometer (BD FACS Canto II, BD Biosciences, USA). The original data were analysed and processed using FlowJo 10.8.1 software.

Cell cycle assay

In this study, flow cytometry was used to determine the effects of different drug treatments on cell cycle arrest using the Cell Cycle Detection Kit (KGA9101-100, KeyGEN, China). The drug treatment protocol was consistent with that of the cell apoptosis detection experiment. Then all cells were fixed with 500 μL of pre-cooled 70 % (*V*/*V*) ethanol and kept at 4 °C for 2 h. Then they were centrifuged at 1500 *g* for 5 min. The supernatant was discarded, and the cells were washed twice with phosphate-buffered saline (PBS). Subsequently, 500 μL of staining working solution containing PI/RNase A (1:9, *V*/*V*) was added, and the mixture was incubated at 37 °C in the dark for 15 min. Then they were detected with the flow cytometer. Their cell cycle phase was analysed using FlowJo 10.8.1 software.

In vivo *anti-lung cancer detection*

LLC tumour-bearing mice were used to detect the antitumour activity of different drugs. C57BL/6J mice were injected subcutaneously with 100 μL LLC cells of 2×10^7 cells mL^{-1} in their right groins. 20 model mice were randomly divided into four groups: the control group, the luteolin group, the piperine group, and the combination group. Two weeks after the subcutaneous injections, the luteolin group, the piperine group, and the combination group were treated intragastrically with luteolin at 50 mg kg^{-1}, piperine at 100 mg kg^{-1}, and luteolin at 50 mg kg^{-1} and piperine at 100 mg kg^{-1}, respectively, every day. The control group was administered an equivalent volume of the blank medium (0.5 % carboxymethyl cellulose sodium, CMC-Na) intragastrically. The administration lasted for 14 days. Their tumour widths and lengths were measured every two days with a vernier calliper. Their tumour volumes were calculated according to Equation *1*.

$$V(\mathrm{mm}^3) = L \times \frac{W^2}{2} \qquad 1$$

where *L* and *W* represent the maximum and minimum diameters, respectively.

The mice were executed on the 14th day. Their lungs, thymuses, livers, and spleens were removed and weighed to calculate organ coefficients. The tumour was weighed, and tumour growth inhibition (TGI) rates were calculated using Equation *2*.

$$\mathrm{TGI}\,(\%) = \left(1 - \frac{RTV_{\mathrm{treatment}}}{RTV_{\mathrm{control}}}\right) \times 100\,\% \qquad 2$$

$RTV_{treatment}$ is defined as the ratio of the tumour volume of the treatment group at the time of measurement to the initial tumour volume of this group. $RTV_{control}$ is defined as the ratio of the tumour volume of the control group at the time of measurement to the initial tumour volume of this group.

In addition, these tumours and lungs were fixed in 4 % paraformaldehyde solution for 24 h. Then they were cut into thin slices and stained with hematoxylin and eosin (HE). Subsequently, they were photographed.

Network pharmacology

To predict the molecular mechanism underlying the synergistic effect of luteolin and piperine, a multi-database integration strategy was adopted. As A549 cells are a classic human lung adenocarcinoma cell line derived from a major subtype of NSCLC, they were selected as the *in vitro* model in this study. Lung adenocarcinoma was selected as the target to obtain representative disease types and ensure consistency between the experimental model and the network pharmacological analysis.

Standardised SMILES strings of luteolin and piperine were retrieved from PubChem (https://pubchem.ncbi.nlm.nih.gov/). Target prediction was conducted *via* SwissTargetPrediction (http://www.swisstargetprediction.ch/) with a probability > 0.1 as the screening threshold. UniPort (Homo sapiens) was used to standardise protein-gene names to identify potential compound targets. Lung adenocarcinoma-associated genes were retrieved from Genecards (https://www.genecards.org/) and the OMIM database (https://www.omim.org/), screened by a relevance score of ≥ 15, and redundant targets were removed to construct a standardised lung adenocarcinoma target library. VENNY 2.1 online tool (https://bioinfogp.cnb.csic.es/tools/venny/) was used to identify common targets between compounds and lung adenocarcinoma targets. Based on these, a component-target network was constructed *via* Cytoscape 3.9.1. A protein-protein interaction (PPI) network was built using the STRING database (https://string-db.org/, Homo sapiens, confidence threshold = 0.4). The topological analysis function of Cytoscape was used to screen core regulatory targets in the PPI network. Common targets were imported into the DAVID database (https://david.ncifcrf.gov/) for Gene Ontology (GO) and Kyoto Encyclopedia of Genes and Genomes (KEGG) pathway enrichment. Fisher's exact test was used to evaluate significance, and statistically significant terms were presented as bar charts and bubble charts to identify core biological processes and key pathways.

Molecular docking

Molecular docking was performed using MOE (version 2019) following established protocols and guidelines (33). The crystal structures of MMP9, EGFR, and SRC were retrieved from the PDB (PDB IDs: 1GKC, 1M14, and 1FMK, respectively). These structures were selected based on moderate to high resolution, intact active sites, presence of co-crystallised ligands, and prior use in docking studies (29–31, 34).

Binding site definition. – The active binding pockets were identified using MOE's Site Finder module, which scans the protein surface based on cavity topology, residue exposure, hydrophobic region distribution, and the binding area of native co-crystallised ligands. For each target, the binding site was defined as the region encompassing the identified pocket centroid (or the co-crystallised ligand).

Protein preparation. – The original crystal structures were imported into MOE. Using the built-in filtering function (35), crystallographic water molecules, native ligands, metal ions, and other irrelevant groups were removed. The Protonate 3D module was then used to add hydrogen atoms, assign atomic charges, and optimise side-chain conformations at pH 7.4. Missing side chains and loop regions were repaired with the Structure Repair module. The protein was energy-minimised using the MMFF94x force field (steepest descent + conjugate gradient) to a convergence of 10^{-4} kcal mol^{-1} Å^{-1} within 10,000 steps.

Ligand preparation. – The 2D structures of piperine and luteolin, as well as the reference ligands (GOL for EGFR, NFH for MMP9, and PTR for SRC), were drawn with ChemDraw 20.0 and converted to 3D in MOE. Geometry optimization and energy relaxation were performed using the MMFF94x force field (convergence 10^{-3} kcal mol^{-1} Å^{-1}, 5,000 steps). Conformers were generated (max 50, energy window 5 kcal mol^{-1}, RMSD 0.5 Å), and the lowest-energy conformer was selected for docking.

Docking protocol. – Docking was performed with the Dock module in semi-flexible mode (ligand flexible, protein rigid). The Triangle Matcher algorithm was used for ligand placement. Initial screening used the London dG scoring function, which accounts for van der Waals forces, hydrogen bonds, hydrophobic interactions, and torsional energy. The top 30 poses were retained, refined, and then rescored with the GBVI/WSA dG scoring function. Final poses were clustered with an RMSD cutoff of 2.0 Å, and the highest-scoring pose from each cluster was retained.

Result analysis. – Docking poses were visualised using PyMOL 2.5.0. Interactions, including hydrogen bonds (2.5–3.5 Å), hydrophobic contacts, and π-π stacking, were analysed. The final binding scores (GBVI/WSA dG) were recorded for each ligand-target pair.

Cross-validation with additional software (PyRx and Discovery Studio). – To ensure reliability, docking was also performed using PyRx (with AutoDock Vina) and Discovery Studio 2020 Client (CDOCKER) (36). The same crystal structures and binding site definitions were used. For PyRx, ligands were prepared from PubChem, optimised with Chem3D (MM2 force field), and processed with AutoDock Tools (adding hydrogens and charges). Proteins were pre-processed with PyMOL to remove water and native ligands. Docking was performed using Vina-2.0; Affinity scores were recorded. According to the literature (37), docking energy values < –4.25 kcal mol^{-1} indicate certain binding activity, < –5.0 kcal mol^{-1} indicate good activity, and < –7.0 kcal mol^{-1} indicate strong binding activity. For Discovery Studio, the CDOCKER protocol (CHARMm force field) was used; CDOCKER_ENERGY scores (more negative = stronger binding) were recorded, which account for van der Waals, electrostatic, hydrogen bond and desolvation terms. Default parameters were applied.

Statistical analysis

GraphPad Prism 10.1.2 (GraphPad, La Jolla, USA) was utilised for all statistical analyses. The numerical data are presented in the form of the mean ± standard deviation (SD). The statistical significance of differences was analysed by unpaired Student's *t*-test (two-group comparisons), one-way ANOVA (three or more groups). Repeated-measure ANOVA was used for repeated-measurement data. Statistical significance was defined as ns (no significance), $p \geq 0.05$, * $p < 0.05$, ** $p < 0.01$, and *** $p < 0.001$.

RESULTS AND DISCUSSION

Effects of piperine and luteolin in inhibiting on cell viability in A549 cells

The synergistic effect of piperine combined with luteolin on A549 cells was evaluated using the MTT assay. As shown in Fig. 1a and 1b, piperine and luteolin significantly inhibited the viability of A549 cells, with the inhibitory effects showing dose- and time-dependence, respectively ($p < 0.05$). Moreover, Table II shows the IC_{50} of luteolin and piperine acting alone on A549 cells at different treatment times. The IC_{50} of luteolin was 108.6, 58.06, and

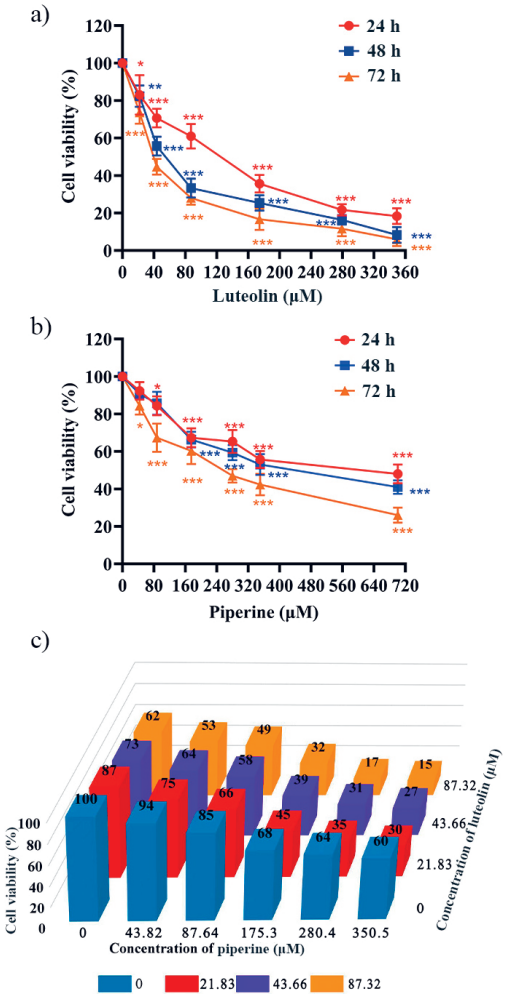

Fig. 1. Cell viability of A549 cells: a) luteolin and b) piperine alone at different concentrations, measured after 24, 48, and 72 h; c) combined treatment (concentrations below the individual 24 h IC_{50} values) after 24 h; $n = 3$, * $p < 0.05$, ** $p < 0.01$, *** $p < 0.001$ (*vs.* medium).

41.85 μmol L^{-1} at 24, 48, and 72 h, respectively. In contrast, those of piperine were 551.8, 418.8, and 243.1 μmol L^{-1} at the same time. In Fig. 1c, the synergistic effects of piperine and luteolin with different concentrations on the viability of A549 cells were determined.

Synergistic inhibitory effect of piperine and luteolin on A549 cells

The synergistic cytotoxic effect of piperine and luteolin on A549 cells was quantitatively assessed. Analysis using CompuSyn software, a widely accepted tool for quantifying drug interactions (*e.g.*, used in the study of cucurbitacin E and myricetin) (38), revealed that all combination index (CI) values ranged from 0.3 to 0.8 (Fig. 2a). According to the Chou-Talalay method, CI < 1 indicates synergy, with lower values indicating stronger effects; thus, the calculated CI range indicates moderate to relatively strong synergistic inhibition. This quantitative synergy was corroborated by cell viability assays, where the combination of 175.3 μmol L^{-1} piperine and 87.32 μmol L^{-1} luteolin resulted in significantly lower cell viability (24.69 %) compared to either agent alone (luteolin 57.73 %; piperine 70.23 %) (Fig. 2b). Morphological observations further supported this enhanced inhibitory effect (Fig. 2c). Together, these data provide robust quantitative and qualitative evidence for the synergistic anti-NSCLC activity of the piperine-luteolin combination.

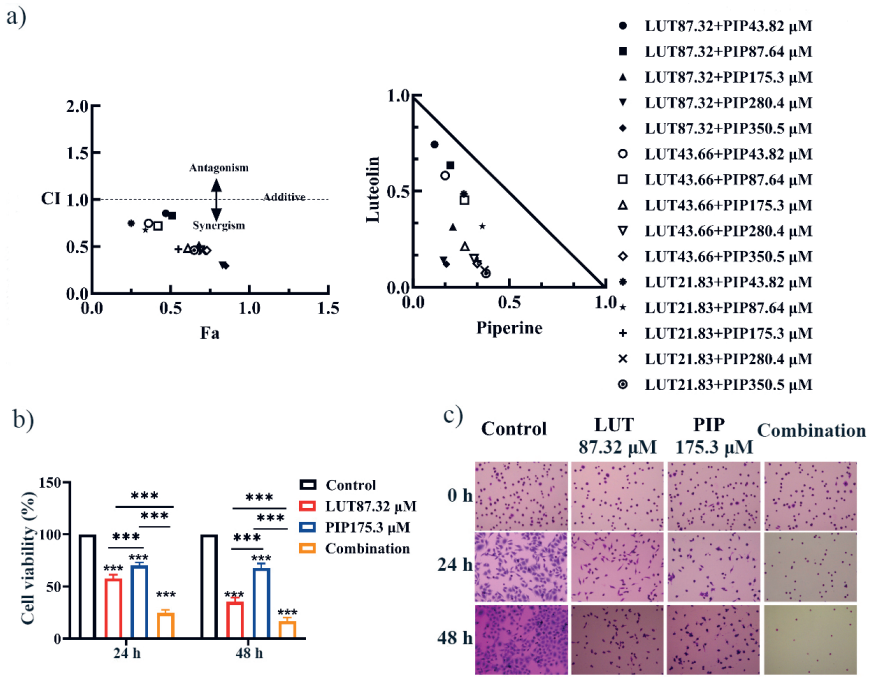

Fig. 2. Cell viability evaluation of the synergistic inhibitory effect of luteolin and piperine on A549 cells: a) Fa-CI curve and normalized concentration scatter plot; b) cell viability and c) cell morphology with luteolin alone (87.32 μmol L^{-1}), piperine alone (175.3 μmol L^{-1}), and the combination of piperine (87.32 μmol L^{-1}) and luteolin (175.3 μmol L^{-1}) treatment for 24 and 48 h on A549 cells; $n = 3$, * $p < 0.05$, ** $p < 0.01$, *** $p < 0.001$ (*vs.* medium).

Synergistic effect of piperine and luteolin in inhibiting wound healing and clone formation on A549 cells

The combination of piperine and luteolin profoundly inhibited the metastatic and proliferative potential of A549 cells. In the wound healing assay, the combination treatment resulted in a significantly larger wound area (Fig. 3a) and markedly lower cell migration rates (17.0 % at 24 h and 22.9 % at 48 h) compared to either agent alone (luteolin 31.8 % and 46.1 %; piperine 36.5 % and 55.5 %) (Fig. 3b). This indicates a superior inhibitory effect on cell migration. Furthermore, the colony formation assay revealed that the combination virtually abolished the long-term clonogenic survival of A549 cells, with minimal colony formation observed (Fig. 3c). The relative colony inhibition rate reached 91.0 %, significantly exceeding that of the luteolin (73.9 %) or piperine (70.8 %) groups (Fig. 3d). These findings, obtained through standard assays essential for evaluating anti-migratory and anti-proliferative efficacy (39), demonstrate that the piperine-luteolin combination not only effectively impedes cell migration but also critically disrupts the self-renewal and proliferative capacity of NSCLC cells.

Synergistic effect of piperine and luteolin in inducing apoptosis and G0/G1 cell cycle arrest in A549 cells

Flow cytometry analysis revealed that the combination of piperine and luteolin significantly enhanced pro-apoptotic and cell cycle arrest effects in A549 cells. The apoptosis

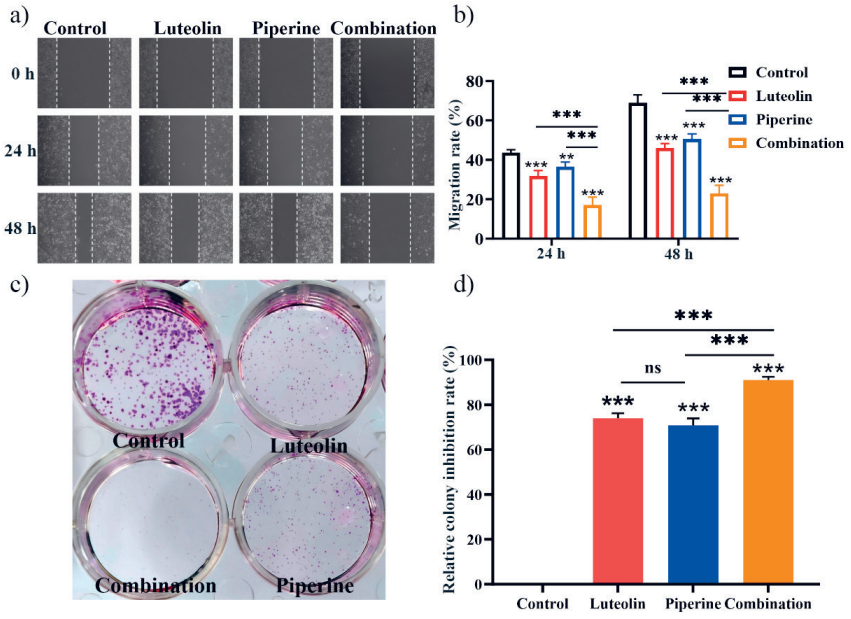

Fig. 3. Wound healing: a) qualitative data; b) quantitative data. Clone formation: c) qualitative data; d) quantitative data. To evaluate the synergistic inhibitory effect of luteolin and piperine on A549 cells cells were treated with luteolin (43.66 μmol L^{-1}), piperine (87.64 μmol L^{-1}), or their combination (43.66 μmol L^{-1} + 87.64 μmol L^{-1}); $n = 3$, * $p < 0.05$, ** $p < 0.01$, *** $p < 0.001$ (*vs.* medium).

rate in the combination group reached 75.60 %, markedly higher than that in the luteolin (24.56 %) or piperine (17.53 %) alone groups (Fig. 4a,b). Given that both compounds individually are known to promote apoptosis (19, 40), this dramatic increase suggests a synergistic potentiation of their intrinsic pro-apoptotic mechanisms.

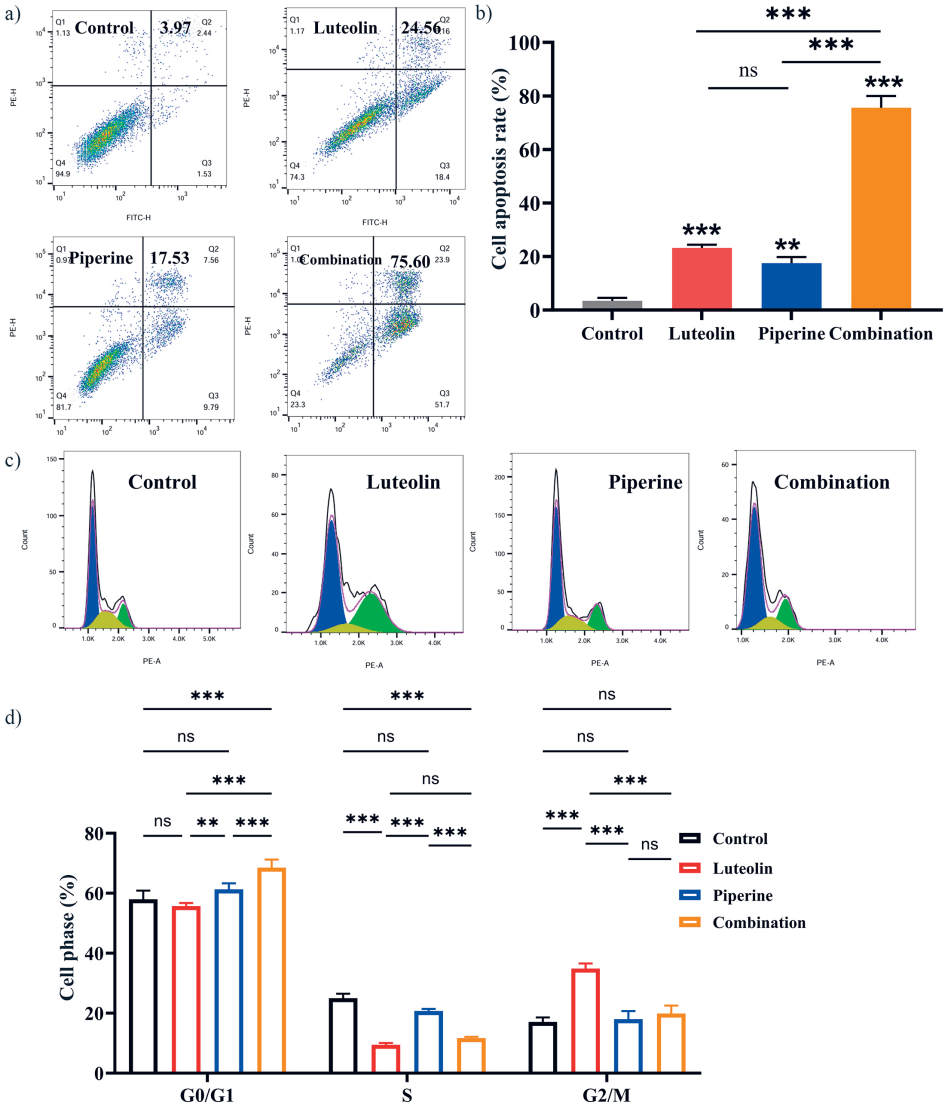

Fig. 4. Cell apoptosis: a) qualitative data; b) quantitative data and cell cycle. Evaluation of the synergistic inhibitory effect of luteolin and piperine on A549 cells: c) qualitative data; d) quantitative data. Cells were treated with luteolin (87.32 μmol L^{-1}), piperine (175.3 μmol L^{-1}), or their combination (87.32 μmol L^{-1} + 175.3 μmol L^{-1}); $n = 3$, * $p < 0.05$, ** $p < 0.01$, *** $p < 0.001$ (*vs.* medium).

Furthermore, the combination induced a distinct cell cycle profile. It caused a pronounced arrest at the G0/G1 phase (68.5 % of cells), compared to luteolin (55.7 %) or piperine (61.3 %) alone (Fig. 4c,d). Notably, this G0/G1 arrest differs from the reported G2/M phase arrest induced by luteolin alone in A549 cells (41). This shift indicates that the presence of piperine may actively participate in and reshape the cell cycle blockade, potentially through the modulation of specific G0/G1 phase-related regulators. The combination of most drugs was verified *in vitro*, which is advantageous for maintaining a relatively constant drug concentration during the experiment (42).

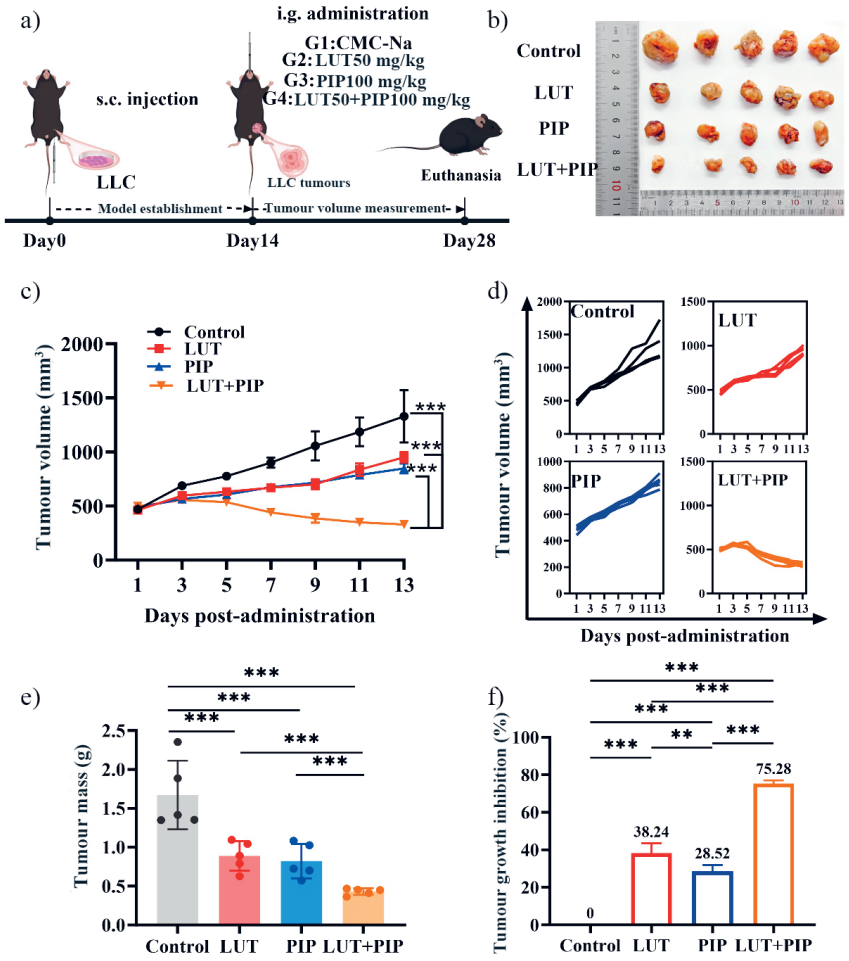

Fig. 5. *In vivo* synergistic effect of luteolin and piperine on inhibiting tumour growth: a) flow chart; b) visual observation of gross tumour tissues; c) dynamic change curve of rough tumour volumes; d) tumour volume of each mouse in each group; e) actual average tumour weight in each group; f) tumour growth inhibition rate (TGI) in each group; $n = 5$, * $p < 0.05$, ** $p < 0.01$, *** $p < 0.001$, LUT – luteolin, PIP – piperine.

Synergistic effect of piperine and luteolin in inhibiting tumour growth in LLC tumour-bearing mice

The LLC tumour-bearing mice were typically used to study *in vivo* efficacy against lung cancer (43). The flowchart is shown in Fig. 5a. Visually, the tumours in the combination group were smaller than those in the piperine, luteolin, or control group in Fig. 5b. There was no statistical difference in body mass among groups, indicating that neither luteolin nor piperine showed obvious toxicity. Tumour growth was significantly inhibited in the combination group. The tumour volume curves (Fig. 5c, d) and the final tumour masses (Fig. 5e) demonstrated the superior efficacy of the combination. The average tumour mass in the combination group (0.429 ± 0.042 g) was substantially lower than in the piperine (0.821 ± 0.222 g), luteolin (0.889 ± 0.189 g), and control (1.672 ± 0.442 g) groups. Consequently, the tumour growth inhibition (TGI) rate for the combination reached 75.28 %, markedly higher than for piperine (28.52 %) or luteolin (38.24 %) alone (Fig. 5f). These results confirm that the combination exerts a synergistic antitumour effect that is not merely the sum superposition of the individual agents.

HE staining of a pathological section is the "gold standard" for observing the morphological changes in tissues and cells, and it is also an indispensable experiment in the evaluation of antitumour efficacy (44). Histopathological evaluation *via* hematoxylin and eosin (HE) staining of subcutaneous tumours (Fig. 6a) revealed that the combination group exhibited lower tumour cell density and more pronounced apoptosis compared to other groups. Furthermore, analysis of lung tissues (Fig. 6b) showed that the combination treatment effectively inhibited metastasis, with minimal tumour cell invasion and a preserved alveolar structure, unlike the single-agent and control groups.

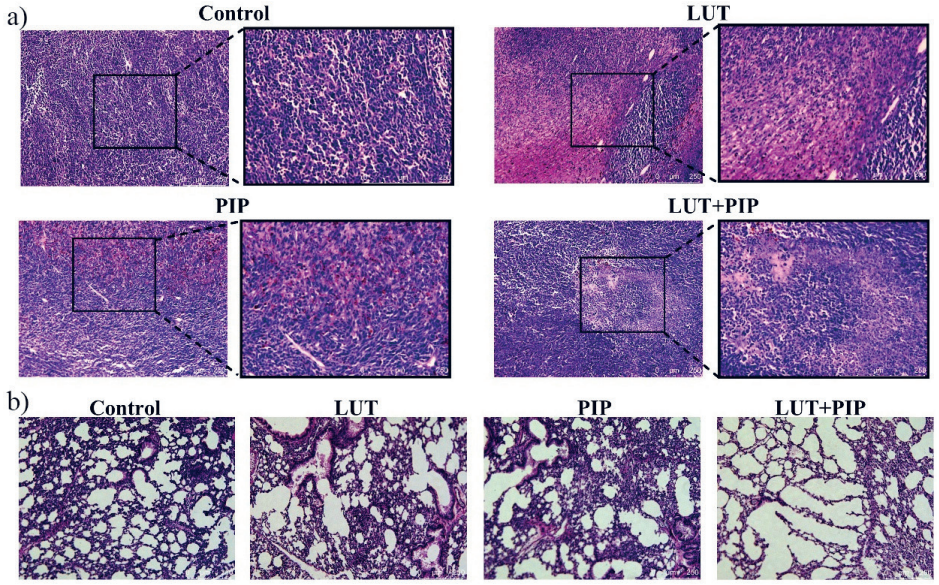

Fig. 6. HE staining results: a) mouse subcutaneous tumour, ×100 and ×200; b) lung tissue, ×100.

Network pharmacology prediction of synergistic targets and pathways of piperine and luteolin against lung adenocarcinoma

It was found that there are 111 predictive targets for luteolin and piperine, as well as 1281 disease-target genes for lung adenocarcinoma. Venn diagram analysis (Fig. 7a) identified 71 overlapping genes, which were defined as the core targets of two compounds acting on lung adenocarcinoma. We further constructed the "component-target" network (Fig. 7b) to visualise their association. AKT1, EGFR, MMP9, SRC, and other core targets were selected through PPI network topology analysis (Fig. 7c), all of which are key regulatory factors in NSCLC. For example, EGFR is a common driver mutation in NSCLC (45).

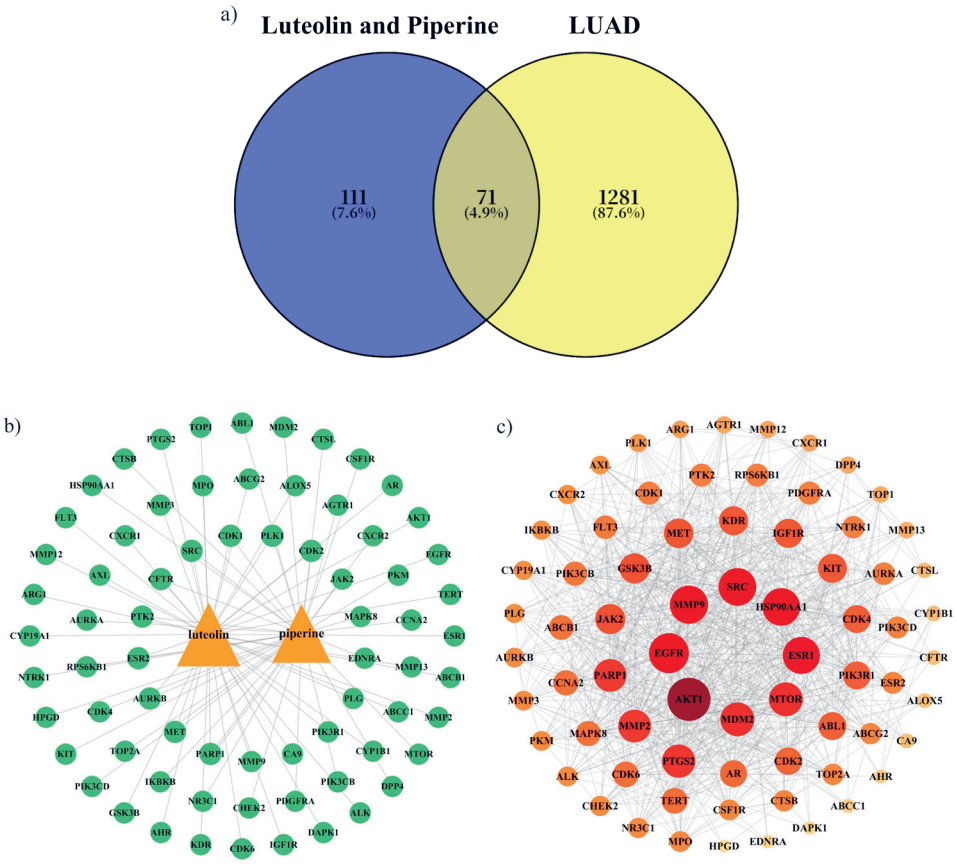

Fig. 7. Network pharmacology analysis diagrams of luteolin and piperine in lung adenocarcinoma (LUAD): a) Venn diagram; b) component-target network diagram; c) PPI network; d) GO enrichment analysis result; e) bubble plot of KEGG pathway analysis. The four target proteins (AKT1, EGFR, SRC, and MMP9) were identified by integrating network topology (hub targets with high centrality), pathological function (regulation of proliferation, invasion, and metastasis), and pathway enrichment (PI3K-Akt and MAPK pathways), along with the availability of crystal structures for docking.

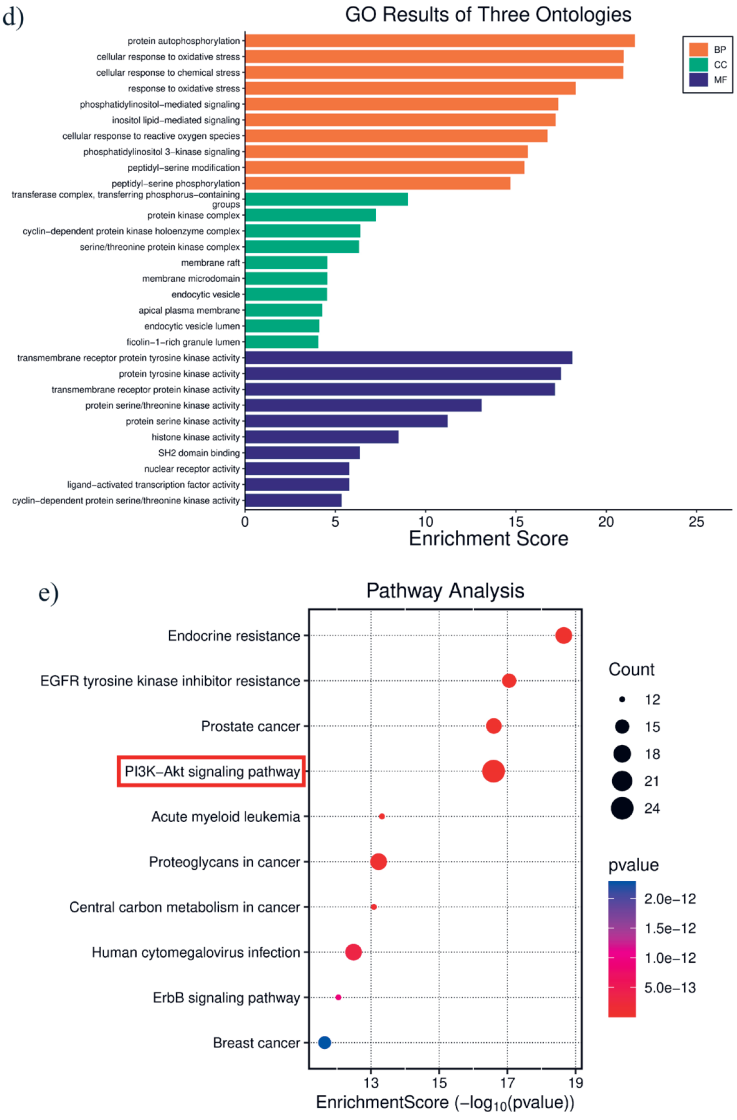

Fig. 7. Continued.

AKT1 is the core molecule of the PI3K/AKT pathway (46). The core targets with high node degree values were screened out based on node degree values, such as AKT1 and EGFR. These proteins are key regulatory factors in the tumour signal pathway. GO enrichment analysis (Fig. 7d) illustrates the core biological processes, cellular components, and molecular functions of the drugs from the biological process (BP), cellular component (CC), and molecular function (MF) dimensions, providing direction for subsequent mechanism

verification. KEGG pathway analysis revealed that the core targets were significantly enriched in the PI3K-AKT signalling pathway (Fig. 7e). This pathway is often aberrantly activated in NSCLC to regulate tumour cell proliferation, apoptosis, and drug resistance (47). This finding is highly consistent with the results of inducing G_0/G_1 phase arrest and promoting apoptosis of A549 cells *in vitro*, suggesting that the PI3K-AKT pathway may be the key pathway of synergistic tumour inhibition.

Table II. Half-maximal inhibitory concentrations (IC_{50}) of luteolin and piperine on A549 cells

Treatment time (h)	IC_{50} of piperine (μmol L^{-1})	IC_{50} of luteolin (μmol L^{-1})
24	551.8	108.6
48	418.8	58.06
72	243.1	41.85

Molecular docking analysis of synergistic targets and mechanisms of piperine and luteolin

Molecular docking using MOE 2019 software was employed to study the interaction characteristics between luteolin, piperine, and 4 core protein targets (Table III). The binding energies of piperine and luteolin to EGFR, MMP9, and SRC were lower than –5 kcal mol^{-1} (Table IV), which met the high-affinity binding standard.

Validation with reference ligands. – To validate the reliability of the docking protocol, the native co-crystallised reference ligands (GOL for EGFR, NFH for MMP9, and PTR for SRC) were re-docked using MOE. The RMSD between the re-docked poses and the crystal ligand conformations was < 2.0 Å for all targets, confirming accurate reproduction of native

Table III. Detailed information on core protein targets for molecular docking

No.	Target	PDB ID	Resolution
1	AKT1	1H10	1.4A
2	EGFR	1M14	2.6A
3	MMP9	1GKC	2.3A
4	SRC	1FMK	1.5A

Table IV. Docking binding energies between active small molecules and target proteins

Component	Binding energy (kcal mol^{-1})			
	AKT1	EGFR	MMP9	SRC
Luteolin	–4.8161	–5.755	–7.1655	–6.2727
Piperine	–5.1486	–6.2585	–7.4117	–5.7445

binding geometry. The calculated binding free energies (GBVI/WSA dG) for the reference ligands and the test compounds are summarised in Table V. The re-docking scores were –3.9 kcal mol^{-1} for EGFR (GOL), –5.4 kcal mol^{-1} for SRC (PTR), and –6.7 kcal mol^{-1} for MMP9 (NFH). Both piperine and luteolin exhibited scores comparable to or lower than the reference ligands, indicating favourable binding affinities.

Table V. Docking scores (GBVI/WSA dG, kcal mol^{-1} of reference ligands, piperine, and luteolin for EGFR, MMP9, and SRC obtained from MOE

Target (PDB ID)	Reference ligand	Reference score	Piperine	Luteolin
EGFR (1M14)	GOL	–3.9	–6.2585	–5.755
MMP9 (1GKC)	NFH	–6.7	–7.4117	–7.1655
SRC (1FMK)	PTR	–5.4	–5.7445	–6.2727

All values are in kcal mol^{-1}. More negative values indicate stronger binding affinity.

Cross-validation using three independent software packages. – To further confirm binding preferences, docking was repeated using PyRx (AutoDock Vina) and Discovery Studio (CDOCKER). The complete set of docking scores from the three software packages is compared in Table VI. PyRx scores ranged from –6.9 to –9.5 kcal mol^{-1}, with both compounds showing the strongest binding to MMP9 (–9.5), followed by EGFR and SRC. PyRx and MOE consistently identified MMP9 as the best target for both compounds (*e.g.*, PyRx: –9.5 kcal mol^{-1} for both; MOE: –7.41 and –7.17 kcal mol^{-1}). Discovery Studio also showed strong binding but amplified luteolin binding to EGFR (–55.37 kcal mol^{-1}) due to its sensitivity to polar

Table VI. Comparison of docking scores (kcal mol^{-1}) for piperine and luteolin against EGFR, MMP9, and SRC using three software packages

Target	Software	Piperine	Luteolin
EGFR	PyRx	–6.9	–7.6
	DS	–25.9918	–55.3717
	MOE	–6.2585	–5.755
MMP9	PyRx	–9.5	–9.5
	DS	–14.1023	–13.1772
	MOE	–7.41	–7.1655
SRC	PyRx	–7.7	–8.4
	DS	–19.01	–34.1569
	MOE	–5.7445	–6.2727

PyRx scores are Affinity (AutoDock Vina); DS scores are CDOCKER_ENERGY; MOE scores are GBVI/WSA dG. All values are in kcal mol^{-1}. More negative values indicate stronger binding affinity. Due to different scoring functions, scores from different software should not be directly compared numerically.

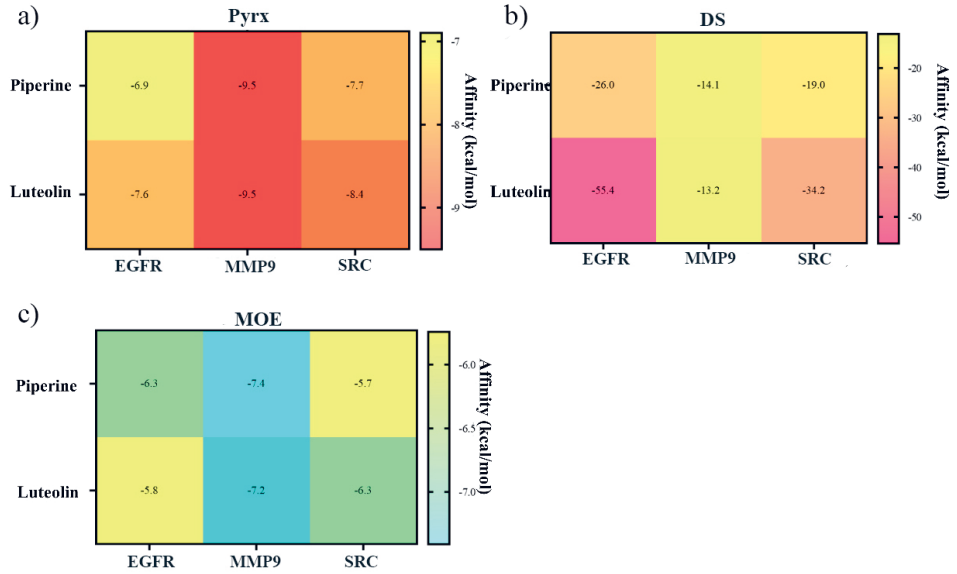

Fig. 8. Docking score heatmaps (kcal mol^{-1}) for piperine and luteolin using: a) PyRx; b) Discovery Studio, and c) MOE. Colour intensity reflects binding strength. Values are provided within each cell.

interactions. The heatmaps in Fig. 8 visually summarise these results. Overall, cross-software comparison confirms that MMP9 is the common core target for both piperine and luteolin. Luteolin exhibits broader binding potential across multiple targets, while piperine shows more specific and stable binding to MMP9. In contrast, SRC did not exhibit consistently strong binding in any of the three software packages, indicating that it is a minor target compared to MMP9.

Overlay of binding poses with reference ligands. – The predicted binding poses of piperine and luteolin overlaid with the co-crystallised reference ligands are shown in Fig. 9. Both compounds occupy the same core active pocket as the reference ligands, further supporting their potential as effective binders.

Detailed interaction analysis. – Piperine and luteolin exhibited a non-overlapping complementary binding mode at the same target (28). Complexes with binding energy (BE) < –5 kcal mol^{-1} were selected and visualised *via* PyMOL 2.6.0. Luteolin interacted with MMP9 mainly *via* hydrogen bonds at Arg^{424}, Ala^{417}, and Glu^{402} (Fig. 10a). Piperine bound to MMP9 *via* a hydrogen bond at Ala^{189}, a different site (Fig. 10b). Regarding EGFR, luteolin established hydrogen bonds with Arg^{835} and Glu^{734} (Fig. 10c), while piperine interacted *via* C–H bonds at Ala^{835} (Fig. 10d). For SRC, luteolin formed hydrogen bonds with Val^{323} and Glu^{339} (Fig. 10e), whereas piperine bound through C–H bond interactions at Gln^{362} (Fig. 10f). This non-overlapping binding mode reduces competition for target binding sites and enhances synergistic inhibition.

It is noted that SwissTargetPrediction suggested that luteolin may bind to all four target proteins (especially MMP9), while piperine showed less evident binding. However,

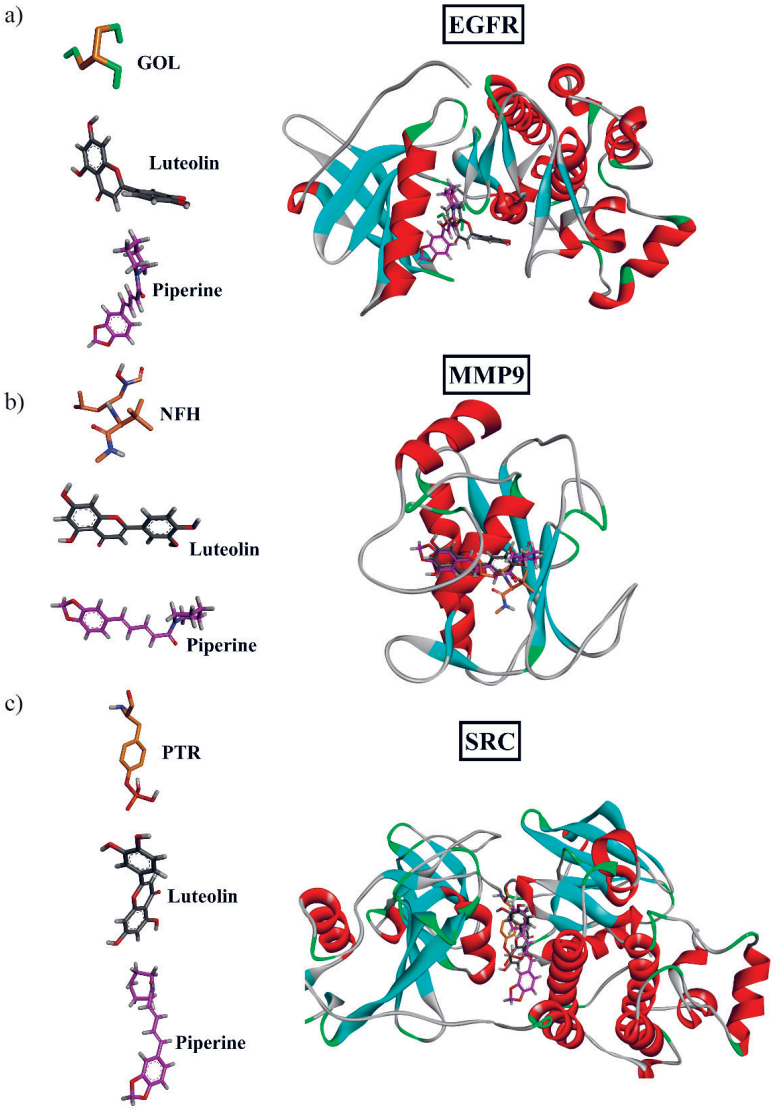

Fig. 9. Overlay of the predicted binding poses of luteolin and piperine with the co-crystallised reference ligands in the active sites of: a) EGFR (PDB: 1M14); b) MMP9 (PDB: 1GKC); c) SRC (PDB: 1FMK). The reference ligands (GOL for EGFR, NFH for MMP9, and PTR for SRC) are shown in yellow. Luteolin and piperine are shown in grey and pink, respectively.

our molecular docking results showed that both compounds had similar docking scores for all targets. This discrepancy is not unexpected, as SwissTargetPrediction and molecular docking operate on different principles and have different focuses (48, 49). SwissTargetPrediction predicts binding possibility based on ligand-target structural simi-

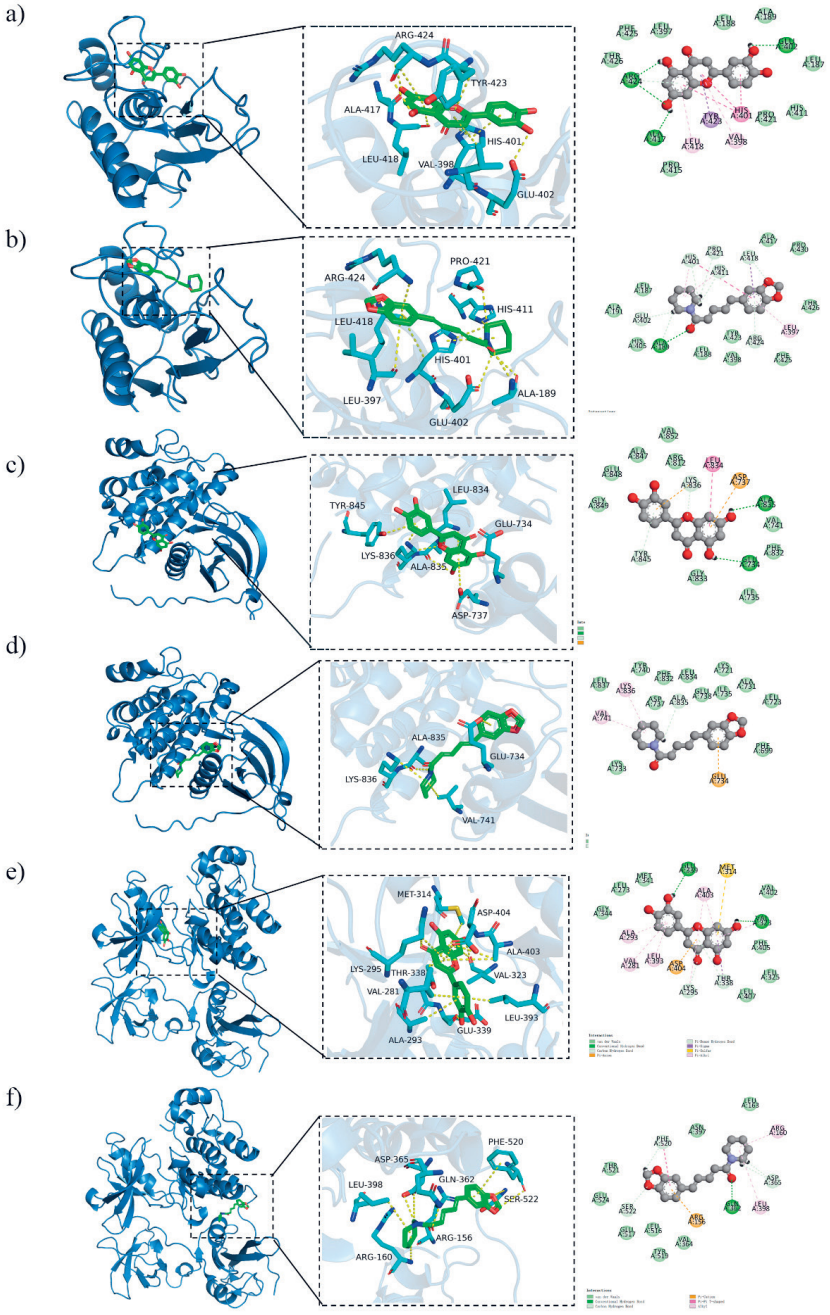

Fig. 10. Molecular docking diagrams of luteolin and piperine with EGFR, MMP9, and SRC; a) luteolin--MMP9; b) piperine-MMP9; c) luteolin-EGFR; d) piperine-EGFR; e) luteolin-SRC; f) piperine-SRC.

larity and cannot quantify binding strength; its results are limited by database completeness. In contrast, our MOE docking is based on the three-dimensional structures of the target proteins and simulates actual binding conformations, providing quantitative binding energy and interaction analysis. Furthermore, the structural features of the two compounds contribute to the difference: luteolin contains multiple polar groups that readily form hydrogen bonds, which are preferentially predicted by SwissTargetPrediction; piperine relies mainly on hydrophobic interactions, which are less recognised by the server but can be accurately quantified by molecular docking. In addition, SwissTargetPrediction is limited by its database (fewer similar ligands for piperine), while our two-stage scoring strategy in MOE mitigates inherent docking scoring limitations. Therefore, the similar docking scores of both compounds are consistent with current understanding.

The results of molecular docking provided direct evidence of the synergistic effect of the two molecules and also laid the foundation for subsequent experimental verification mechanisms, such as Western blot and gene knockout.

Study limitations

Several limitations should be noted. First, the LLC model, though widely used, is a murine tumour and does not fully capture the genetic and immune features of human NSCLC. Our *in vivo* findings, therefore, have limited translational relevance (50). The observed synergy in LLC-bearing mice should be seen as a proof-of-concept in a syngeneic system, not a direct indicator of clinical efficacy. More clinically relevant models, such as PDX or GEMMs, are needed for further validation (51).

Second, pharmacokinetic studies have reported a C_{max} of piperine of approximately 0.983 μg mL^{-1} after oral administration in rats, and a C_{max} of luteolin of approximately 3.04 μg mL^{-1} in rats (52, 53), yet the concentrations used in our synergy assays (piperine 175.3 μmol L^{-1}, luteolin 87.32 μmol L^{-1}) exceed these plasma levels. Nevertheless, they were selected below the individual IC_{50} values according to the Chou-Talalay method to determine the combination index. Our findings should be interpreted as a mechanistic proof of concept. Future bioavailability-enhancing strategies, including nanoformulation, could help translate this synergy into *in vivo* settings (54).

Third, this study focused on establishing the synergistic anti-proliferative efficacy of the piperine-luteolin combination in cancer cells and did not assess cytotoxicity against normal cell lines. Therefore, the selectivity index (SI), a key metric for evaluating the therapeutic window, could not be determined. This constitutes an important aspect for future translational studies, which will be essential to fully characterise the safety profile of this promising combination.

CONCLUSIONS

In conclusion, it was systematically confirmed that luteolin and piperine have synergistic antitumour effects on NSCLC *in vitro* and *in vivo* by A549 cells and LLC tumour-bearing mice. Network pharmacology and multi-software molecular docking (including reference ligand validation) identified EGFR, MMP9, SRC, and the PI3K/AKT pathway as key mediators, with MMP9 as the common core target, providing structural support for the synergy. The combination of piperine and luteolin had a highly effective tumour-inhibi-

tory effect at low concentrations. It provided an experimental basis for the clinical application of the combined strategy of natural products.

Acknowledgements. – The authors gratefully acknowledge Prof. Tian Chang for the generous gift of the A549 cell line used in this research.

Conflict of Interest. – The authors declare there are no competing interests.

Funding. – This project was funded by Anhui University Natural Science Research Projects of China (grant number KJ2019A0097), Introduction of Talent Fund Project of Anhui University of Science and Technology (grant number 11079), and the open foundation of Key Laboratory of Tropical Plant Resource Chemistry of Hainan Province (grant number rdzw2025s04).

Author's contribution. – Methodology, A.G.; analysis, Y.L.; investigation, L.W. and B.W.; validation, L.W., B.W., and Y. L.; data curation, Y.D.; writing, original draft preparation, L.W.; writing, review and editing, Y.C.; supervision, Y.C.; project administration, F.J.; funding acquisition, Y.C. All authors have read and agreed to the published version of the manuscript.

REFERENCES

1. H. Sung, J. Ferlay, R. L. Siegel, M. Laversanne, I. Soerjomataram, A. Jemal and F. Bray, Global cancer statistics 2020: GLOBOCAN estimates of incidence and mortality worldwide for 36 cancers in 185 countries, *CA Cancer J. Clin.* **71**(3) (2021) 209–249; https://doi.org/10.3322/caac.21660
2. J. J. Shi, Y. C. Chen, C. T. Peng, L. W. Kuang, Z. T. Zhang, Y. K. Li and K. Huang, Advances in targeted therapy against driver mutations and epigenetic alterations in non-small cell lung cancer, *Oncologie* **24**(4) (2022) 613–648; https://doi.org/10.32604/oncologie.2022.027545
3. H. Y. Guo, J. Zhang, C. Qin, H. Yan, T. Liu, H. Y. Hu, S. J. Tang, S. J. Tang and H. N. Zhou, Biomarker-targeted therapies in non-small cell lung cancer: Current status and perspectives, *Cells* **11**(20) (2022) Article ID 3200 (24 pages); https://doi.org/10.3390/cells11203200
4. L. Ni and L. Nie, Mechanisms of resistance to the third-generation epidermal growth factor receptor-tyrosine kinase inhibitors in non-small cell lung cancer, *Chin. J. Lung Cancer*, **21**(2) (2018) 110–115; https://doi.org/10.3779/j.issn.1009-3419.2018.02.02
5. A. Malhotra, P. Nair and D. K. Dhawan, Study to evaluate molecular mechanics behind synergistic chemopreventive effects of curcumin and resveratrol during lung carcinogenesis, *PloS ONE* **9**(4) (2014) e93820; https://doi.org/10.1371/journal.pone.0093820
6. A. Alemi, M. H. Karamallah, M. Sabaghan, S. A. Hosseini, A. Veisi, S. H. Karamallah and M. Farokhifar, Combination drug therapy by herbal nanomedicine prevent multidrug resistance protein 1: Promote apoptosis in lung carcinoma, *J. Appl. Biomater. Functional Materials* **22** (2024) (15 pages); https://doi.org/10.1177/22808000241235442
7. M. T. Zhu, Y. P. Sun, Y. Su, W. Guan, Y. Wang, J. W. Han, S. Wang, B. Y. Yang, Q. H. Wang and H. X. Kuang, Luteolin: A promising multifunctional natural flavonoid for human diseases, *Phytother. Res.* **38**(7) (2024) 3417–3443; https://doi.org/10.1002/ptr.8217
8. N. Aziz, M. Y. Kim and J. Y. Cho, Anti-inflammatory effects of luteolin: A review of in vitro, in vivo, and in silico studies, *J. Ethnopharmacology* **225**(2018) 342–358; https://doi.org/10.1016/j.jep.2018.05.019
9. H. Slika, H. Mansour, N. Wehbe, S. A. Nasser, R. Iratni, G. Nasrallah, A. Shaito, T. Ghaddar, F. Kobeissy and A. H. Eid, Therapeutic potential of flavonoids in cancer: ROS-mediated mechanisms, *Biomed. Pharmacother.* **146**(2022) Article ID 112442 (18 pages); https://doi.org/10.1016/j.biopha.2021.112442

10. M. D. D. Chagas, C. J. M. Tellis, A. R. Silva, M. Brito, A. J. Teodoro, M. D. Elias, S. R. Ferrarini, M. D. Behrens and C. F. Goncalves-de-Albuquerque, Luteolin: A novel approach to fight bacterial infection, *Microbial Pathogenesis* **204** (2025) Article ID 107519; https://doi.org/10.1016/j.micpath.2025.107519
11. Z. Y. Wang, M. M. Zeng, Z. J. Wang, F. Qin, J. Chen and Z. Y. He, Dietary Luteolin: A narrative review focusing on its pharmacokinetic properties and effects on glycolipid metabolism, *J. Agricult. Food Chem.* **69**(5) (2021) 1441–1454; https://doi.org/10.1021/acs.jafc.0c08085
12. K. Rakoczy, J. Kaczor, A. Soltyk, N. Szymanska, J. Stecko, J. Sleziak, J. Kulbacka and D. Baczynska, Application of luteolin in neoplasms and nonneoplastic diseases, *Int. J. Mol. Sci.* **24**(21) (2023) Article ID 15995 (34 pages)https://doi.org/10.3390/ijms242115995
13. J. Lu, G. L. Li, K. F. He, W. Q. Jiang, C. Xu, Z. Q. Li, H. H. Wang, W. B. Wang, H. Y. Wang, X. D. Teng and L. S. Teng, Luteolin exerts a marked antitumour effect in cMet-overexpressing patient--derived tumour xenograft models of gastric cancer, *J. Translat. Med.* **13** (2015) Article ID 42 (11 pages); https://doi.org/10.1186/s12967-015-0398-z
14. A. K. Pandurangan and N. M. Esa, Luteolin, a bioflavonoid inhibits colorectal cancer through modulation of multiple signaling pathways: A review, *Asian Pacific J. Cancer Prev.* **15**(14) (2014) 5501–5508; https://doi.org/10.7314/apjcp.2014.15.14.5501
15. H. T. Wu, J. Lin, Y. E. Liu, H. F. Chen, K. W. Hsu, S. H. Lin, K. Y. Peng, K. J. Lin, C. C. Hsieh and D. R. Chen, Luteolin suppresses androgen receptor-positive triple-negative breast cancer cell proliferation and metastasis by epigenetic regulation of MMP9 expression via the AKT/mTOR signaling pathway, *Phytomedicine* **81** (2021) Article ID 153437 (12 pages); https://doi.org/10.1016/j.phymed.2020.153437
16. J. X. Ma, J. G. Mo, Y. F. Feng, L. Z. Wang, H. Jiang, J. M. Li and C. Jin, Combination of transcriptomic and proteomic approaches helps unravel the mechanisms of luteolin in inducing liver cancer cell death via targeting AKT1 and SRC, *Front. Pharmacol.* **15** (2024) Article ID 1450847 (19 pages); https://doi.org/10.3389/fphar.2024.1450847
17. Z. B. Jiang, W. J. Wang, C. Xu, Y. J. Xie, X. R. Wang, Y. Z. Zhang, J. M. Huang, M. Huang, C. Xie, P. Liu, X. X. Fan, Y. P. Ma, P. Y. Yan, L. Liu, X. J. Yao, Q. B. Wu and E. L. H. Leung, Luteolin and its derivative apigenin suppress the inducible PD-L1 expression to improve anti-tumour immunity in KRAS-mutant lung cancer, *Cancer Lett.* **515** (2021) 36–48; https://doi.org/10.1016/j.canlet.2021.05.019
18. G. M. Meng, K. Q. Chai, X. D. Li, Y. Q. Zhu and W. H. Huang, Luteolin exerts pro-apoptotic effect and anti-migration effects on A549 lung adenocarcinoma cells through the activation of MEK/ERK signaling pathway, *Chemico-Biological Interactions* **257** (2016) 26–34; https://doi.org/10.1016/j.cbi.2016.07.028
19. H. Li, Z. Qiu, W. Xu, X. Chen, D. Wei and Y. Wang, Luteolin inhibits proliferation of lung cancer A549 cells by increasing ROS production and inhibiting the AKT/mTOR signaling pathway and HO-1 expression, *Nan Fang Yi Ke Da Xue Xue Bao* **44**(12) (2024) 2367–2374; https://doi.org/10.12122/j.issn.1673-4254.2024.12.12
20. J. Remon, C. E. Steuer, S. S. Ramalingam and E. Felip, Osimertinib and other third-generation EGFR TKI in EGFR-mutant NSCLC patients, *Ann. Oncology* **29** (2018) I20-I27; https://doi.org/10.1093/annonc/mdx704
21. S. Baldacci, E. J. Brea, F. Facchinetti, Z. Li, K. Ngo, S. Malhotra, M. A. Booker, M. Y. Tolstorukov, S. Chakravarti, C. Hinchey, N. R. Mahadevan, F. Lococo, S. D'Agnelli, L. Gnetti, N. Campanini, A. Leonetti, W. W. Feng, J. A. Tsai, A. V. Hartley, M. A. Locquet, L. Fournel, M. Alifano, A. Mansuet-Lupo, A. Saldanha, W. Haller, L. M. Zasadil, M. Zielinska, K. Bui, B. Tuladhar, P. H. Lizotte, E. V. Ivanova, L. V. Sequist, P. C. Gokhale, C. P. Paweletz, E. L. Smith, P. A. Janne and D. A. Barbie, Eradicating drug tolerant persister cells in EGFR-mutated non-small cell lung cancer by targeting TROP2 with CAR-T cellular therapy, *Cancer Discov.* **15**(11) (2025) 2235–2250; https://doi.org/10.1158/2159-8290.Cd-24-1515

22. B. C. Tong, L. Gu, X. F. Wang, D. A. Wigle, J. D. Phillips, D. H. Harpole, Jr., J. A. Klapper, T. Sporn, N. E. Ready and T. A. D'Amico, Perioperative outcomes of pulmonary resection after neoadjuvant pembrolizumab in patients with non-small cell lung cancer, *J. Thoracic Cardiovasc. Surgery* **163**(2) (2022) 427–436; https://doi.org/10.1016/j.jtcvs.2021.02.099

23. H. Abolhassani, M. S. Safavi, S. Handali, M. Nosrati and S. A. Shojaosadati, Synergistic effect of self-assembled curcumin and piperine co-loaded human serum albumin nanoparticles on suppressing cancer cells, *Drug Devel. Ind. Pharm.* **46**(10) (2020) 1647–1655; https://doi.org/10.1080/03639045.2020.1820032

24. M. K. Pal, S. P. Jaiswar, A. K. Srivastav, S. Goyal, A. Dwivedi, A. Verma, J. Singh, A. K. Pathak, P. L. Sankhwar and R. S. Ray, Synergistic effect of piperine and paclitaxel on cell fate via cyt-c, Bax/Bcl-2-caspase-3 pathway in ovarian adenocarcinomas SKOV-3 cells, *Eur. J. Pharmacol.* **791** (2016) 751–762; https://doi.org/10.1016/j.ejphar.2016.10.019

25. D. Chen, Y. M. Ma, Z. Y. Guo, L. Liu, Y. R. Yang, Y. R. Wang, B. N. Pan, L. Y. Wu, Y. Y. Hui and W. J. Yang, Two natural alkaloids synergistically induce apoptosis in breast cancer cells by inhibiting STAT3 activation, *Molecules* **25**(1) (2020) Article ID 216 (16 pages); https://doi.org/10.3390/molecules25010216

26. M. K. Manickasamy, A. Kumar, B. Bharathwajchetty, M. S. Alqahtani, M. Abbas, A. Alqahtani, J. Unnikrishnan, A. Bishayee, G. Sethi and A. B. Kunnumakkara, Synergistic enhancement: Exploring the potential of piperine in cancer therapeutics through chemosensitization and combination therapies, *Life Sci.* **354** (2024) Article ID 122943; https://doi.org/10.1016/j.lfs.2024.122943

27. Y. Liu, X. Li, C. Chen, N. Ding, S. Ma and M. Yang, Exploration of compatibility rules and discovery of active ingredients in TCM formulas by network pharmacology, *Chin. Herb. Med.* **16**(4) (2024) 572–588; https://doi.org/10.1016/j.chmed.2023.09.008

28. R. Jakhar, M. Dangi, A. Khichi and A. K. Chhillar, Relevance of molecular docking studies in drug designing, *Curr. Bioinformatics* **15**(4) (2020) 270–278; https://doi.org/10.2174/1574893615666191219094216

29. X. Li, J. Sun, X. Li, Y. Dai, C. Zhao, S. Man, Y. Wang and W. Gao, Dioscin-6′-*O*-acetate impairs migration of lung cancer cells through attenuations of MMP-2 and MMP-9 via NF-κB suppression, *Med. Chem. Res.* **28**(1) (2019) 1–12; https://doi.org//10.1007/s00044-018-2257-y

30. I. Aggarwal, R. B. Aniyery, A. Gupta, H. Kaur, Megha, Diksha and S. Sudheer, *Anticancer and Antimicrobial Studies of Dibutyl(hexadecanoyloxy)stannyl Hexadecanoate*, in *Emerging Trends in Synthesis and Catalysis*, Springer, New York 2023, pp. 13–33.

31. A. H. Jumaa, I. M. Hade, K. N. Abdulla and Y. S. Yasin, Ciprofloxacin and metformin as dual therapeutic agents: Synergistic impact on cervical cancer cell line proliferation: Insight into cytoplasmic SRC tyrosine kinase targeting, *Asian Pacific J. Cancer Biol.* **10**(3) (2025) 699–712; https://doi.org/10.31557/apjcb.2025.10.3.699-712

32. T. C. Chou, Drug combination studies and their synergy quantification using the Chou-Talalay method, *Cancer Res.* **70**(2) (2010) 440–446; https://doi.org/10.1158/0008-5472.Can-09-1947

33. F. D. Prieto-Martínez, M. Arciniega and J. L. Medina-Franco, Molecular docking: Current advances and challenges, *TIP Revista Especializada en Ciencias Químico-Biológicas* **21**(suppl 1) (2018) 65–87; https://doi.org/10.22201/fesz.23958723e.2018.0.143

34. A. Sailapathi, G. Murugan, K. Somarathinam, S. Gunalan, R. Jagadeesan, N. Yoosuf, S. Kanagaraj and G. Kothandan, Proposing the promiscuous protein structures in JNK1 and JNK3 for virtual screening in pursuit of potential leads, *ACS Omega* **5**(8) (2020) 3969–3978; https://doi.org/10.1021/acsomega.9b03458

35. S. Vilar, G. Cozza and S. Moro, Medicinal chemistry and the molecular operating environment (MOE): Application of QSAR and molecular docking to drug discovery, *Curr. Topics Med. Chem.* **8**(18) (2008) 1555–1572; https://doi.org/10.2174/156802608786786624

36. G. Wu, D. H. Robertson, C. L. Brooks, 3rd and M. Vieth, Detailed analysis of grid-based molecular docking: A case study of CDOCKER-A CHARMm-based MD docking algorithm, *J. Comput. Chem.* **24**(13) (2003) 1549–1562; https://doi.org/10.1002/jcc.10306

37. S. Gautam, In silico drug development against RNA dependent RNA polymerase of SARS-CoV-2, M.Sc. Thesis, Central Department of Biotechnology, Tribhuvan University, Kirtipur, Kathmandu, Nepal, 2023; https://hdl.handle.net/20.500.14540/23764

38. J. F. Zhang, B. Aray, Y. Zhang, Y. L. Bai, T. Yuan, S. L. Ding, Y. Y. Xue, X. L. Huang and Z. Y. Li, Synergistic effect of cucurbitacin E and myricetin on anti-non-small cell lung cancer: Molecular mechanism and therapeutic potential, *Phytomedicine* **111** (2023) Article ID 154619; https://doi.org/10.1016/j.phymed.2022.154619

39. Q. Zhang, Y. Zhou, X. Y. Feng, Y. Gao, C. Z. Huang and X. Q. Yao, Low-dose orlistat promotes the therapeutic effect of oxaliplatin in colorectal cancer, *Biomed. Pharmacother.* **153** (2022) Article ID 113426 (12 pages); https://doi.org/10.1016/j.biopha.2022.113426

40. Y. Lin, J. P. Xu, H. H. Liao, L. Li and L. Pan, Piperine induces apoptosis of lung cancer A549 cells via p53-dependent mitochondrial signaling pathway, *Tumour Biol.* **35**(4) (2014) 3305–3310; https://doi.org/10.1007/s13277-013-1433-4

41. X. T. Cai, T. M. Ye, C. Liu, W. G. Lu, M. Lu, J. Zhang, M. Wang and P. Cao, Luteolin induced G2 phase cell cycle arrest and apoptosis on non-small cell lung cancer cells, *Toxicol. in Vitro* **25**(7) (2011) 1385–1391; https://doi.org/10.1016/j.tiv.2011.05.009

42. T. C. Chou, Theoretical basis, experimental design, and computerized simulation of synergism and antagonism in drug combination studies, *Pharmacol. Rev.* **58**(3) (2006) 621–681; https://doi.org/10.1124/pr.58.3.10

43. Y. R. Wang, J. J. Xiao, X. M. Dong, S. C. Meng, S. J. Deng, B. Kuang, J. Yan, F. Zhao and H.-H. Zeng, The antitumour activity of Shuang-Xi-Zuo-Wan-1 in C57/BL mice, *J. Peking University Health Sciences* **37**(4) (2005) 421–424.

44. A. H. Fischer, K. A. Jacobson, J. Rose and R. Zeller, Hematoxylin and eosin staining of tissue and cell sections, *Cold Spring Harb. Protoc.* **2008** (2008) pdb.prot4986; https://doi.org/10.1101/pdb.prot4986

45. X. F. Li, S. X. Ren, C. Zhao, J. Y. Li, G. H. Yang, W. He and C. C. Zhou, Quantitative test of mutant EGFR and its effect on efficacy of EGFR TKI in advanced NSCLC, *J. Thorac Oncol.* **8** (2013) S787–S787; https://doi.org/10.1200/jco.2013.31.15_suppl.e22186

46. M. W. Lee, D. S. Kim, N. Y. Min and H. T. Kim, Akt1 inhibition by RNA interference sensitizes human non-small cell lung cancer cells to cisplatin, *Int. J. Cancer* **122**(10) (2008) 2380–2384; https://doi.org/10.1002/ijc.23371

47. H. Cheng, M. Shcherba, G. Pendurti, Y. Liang, B. Piperdi and R. Perez-Soler, Targeting the PI3K/AKT/mTOR pathway: Potential for lung cancer treatment, *Lung Cancer Manag.* **3**(1) (2014) 67–75; https://doi.org/10.2217/lmt.13.72

48. D. Gfeller, A. Grosdidier, M. Wirth, A. Daina, O. Michielin and V. Zoete, SwissTargetPrediction: A web server for target prediction of bioactive small molecules, *Nucleic Acids Res.* **42**(W1) (2014) W32-W38; https://doi.org/10.1093/nar/gku293

49. M. Karadag-Alpaslan, *Molecular Docking*, in *International Studies and Evaluations in the Field of Health Sciences,* (Ed. H. Akgül, E. Şahna, Z. Selamoğlu), Chapter 8, Ondokuz Mayis University, Samsun 2024, pp. 105–113.

50. W. L. Shang, C. H. Lai, S. W. Luo and L. M. Chen, Murine models of lung adenocarcinoma: Valuable tools for preclinical investigation, *Gene* **971** (2025) Article ID 149802; https://doi.org/10.1016/j.gene.2025.149802

51. N. Lonberg, The problem with syngeneic mouse tumour models, *Cancer Immunol. Res.* **13**(4) (2025) 456–462; http://doi.org/10.1158/2326-6066.Cir-24-1046

52. P. K. Sahu, A. Sharma, S. Rayees, G. Kour, A. Singh, M. Khullar, A. Magotra, S. K. Paswan, M. Gupta, I. Ahmed, S. Roy, M. Kumar Tikoo, S. L. Sharma, S. Singh and G. Singh, Pharmacokinetic

study of piperine in Wistar rats after oral and intravenous administration, *Int. J. Drug Deliv.* **6**(1) (2014) 82–87; http://www.arjournals.org/index.php/ijdd/index

53. X. X. Dong, W. Lan, X. B. Yin, C. J. Yang, W. P. Wang and J. Ni, Simultaneous determination and pharmacokinetic study of quercetin, luteolin, and apigenin in rat plasma after oral administration of *Matricaria chamomilla* L. extract by HPLC-UV, *Evidence-Based Complement. Alter. Med*. **2017** (2017) Article ID 8370584 (7 pages); https://doi.org/10.1155/2017/8370584
54. G. Kumar, B. Ruivinho, T. Virmani, P. Brandao, P. Choudhary, N. Kumar Chouhan, M. Kumar, A. Sharma, M. S. Akhtar, O. Afzal, S. Farooqui, S. O. D. Duarte and P. Fonte, Unlocking the full potential of piperine-loaded nanocarriers for cancer treatment, *Therap. Del.* **16**(9) (2025) 881–901; https://doi.org/10.1080/20415990.2025.2542107